Experimental Mechanics (2009) 49:511–522
DOI 10.1007/s11340-008-9198-1

Quantitative Impact Testing of Energy Dissipation at Surfaces

G. Constantinides · C.A. Tweedie · N. Savva · J.F. Smith · K.J. Van Vliet

Received: 9 November 2007 / Accepted: 17 October 2008 / Published online: 2 December 2008

Abstract Impact testing with nanoscale spatial, force, and temporal resolution has been developed to address quantitatively the response of surfaces to impingement of local contact at elevated velocities. Here, an impact is generated by imparting energy to a pendulum carrying an indenter, which then swings towards a specimen surface. The pendulum displacement as a function of time $x(t)$ is recorded, from which one can extract the maximum material penetration $x_{\max}$, residual deformation x_r, and indentation durations t_{in} and t_{out}. In an inverse application one can use the $x(t)$ response to extract material constants characterizing the impact deformation and extent of energy absorption, including material specific resistance coefficient C_{in}, coefficient of restitution e, and dynamic hardness H_{imp}. This approach also enables direct access to the ratio H/E, or resilience of the deformed material volume, at impact velocities of interest. The impact response of aluminum was studied for different contact velocities, and the mechanical response was found to correlate well with our one-dimensional contact model. Further experiments on annealed and work hardened gold showed that dynamic hardness H_{imp} scales with contact velocity and highlighted the importance of rate-dependent energy absorption mechanisms that can be captured by the proposed experimental approach.

Keywords Nanoindentation · Impact · Dynamic hardness · Coefficient of restitution · Energy dissipation

G. Constantinides · C.A. Tweedie · K.J. Van Vliet (✉, SEM member)
Department of Materials Science and Engineering, Massachusetts Institute of Technology, Cambridge, MA 02139, USA
e-mail: krystyn@mit.edu

N. Savva
Department of Mathematics, Massachusetts Institute of Technology, Cambridge, MA 02139, USA

G. Constantinides
Department of Mechanical Engineering and Materials Science and Engineering, Cyprus University of Technology, Lemesos, Cyprus

J.F. Smith
Micro Materials, Ltd, Wrexham, UK

Introduction

Technologically important coating and device length scales have shifted to the submicron regime, increasing demand for nanoscale analysis of critical properties. Instrumented indentation [1–3] and atomic force microscopy (AFM) [4] techniques have become ubiquitous tools for mechanical characterization of material surfaces and small volumes with nanoscale resolution of depth and force. These techniques, however, are primarily restricted to the quasi-static regime of loading rates. Small-scale impact testing of materials has been recently reported, although this has been essentially qualitative in nature, such as the number of repetitive impacts to induce fatigue failure of coatings [5]. This paper presents a new experimental approach and analysis that quantitatively evaluates the mechanical energy dissipation of materials subjected to contact impacts over nano- to micro- scale penetration depths. Deformation and damage of material surfaces under rapid localized

contact is encountered in diverse fields ranging from solid particle erosion, manufacturing processes, shot peening, and accidental impacts of fragmented projectiles. Therefore, the new experimental approach described herein has considerable practical significance in the prediction and design of material surfaces that absorb and dissipate energy upon mechanical impact.

The application of energetic impacts to characterize mechanical behavior and properties of materials [6–10] was enabled by the analytical solutions of elastic contact and elastic wave propagation in semi-infinite solids by Hertz [11] and Saint Venant [12]. In fact, the experimental origins of impact characterization can be traced to scleroscopy, a simple but largely defunct experimental approach developed in the 1900s, in which a conical diamond indenter is dropped from a fixed height onto the material of interest, and the rebound height is measured to infer the impact resistance on an arbitrary scale (Shore units); naturally, materials of greater impact resistance exhibit greater rebound heights [13]. Such experimental studies of impact deformation and energy absorption were confined to materials of macroscale physical dimensions, due chiefly to technological limitations in accurate measurement of position, displacement, and force.

Currently, instrumentation for contact-based deformation of nanoscale resolution is widely available, and has enabled both general mechanical characterization of small material volumes (e.g., thin films adhered to substrates [14–16] and free-standing nanowires [17, 18]) as well as unprecedented access to the physics of deformation processes such as dislocation nucleation in crystals [19–24]. Here, we extend these techniques to impact indentation, as distinct from quasi-static loading/unloading cycles. We show that this impact response and analysis can complement macroscopic dynamic testing in the low impact velocity regime (mm/s). The main advantages of this technique lie in its analytical simplicity and ease of implementation to quantify energy absorption of a material surface and/or nano- to micro-scale material volume. Thus, this approach is amenable to the quantification of impact responses in structurally heterogeneous materials including films and composites.

Impact Experimental Design

Impact Apparatus

Figure 1(a) outlines the operating principles of the experimental apparatus. The load frame comprises a commercially available instrumented indenter (NanoTest, Micro Materials, Wrexham, UK), which is a pendulum-based device in which load is applied and measured through actuation of the pendulum around a frictionless pivot (where internal friction is considered negligible for the small displacements and steel spring material used) via an electromagnetic voice coil; displacement of the indenter during load application is measured via a capacitive transducer mounted on the lower end of the pendulum. For the experiments discussed below, a three-sided pyramid with face angles of 65.3° composed of diamond, commonly referred to as Berkovich indenter, was used. Both force and displacement are independently calibrated and thermally stable, and the entire instrument is housed within an acoustic isolation enclosure at controlled temperature (26°C) and

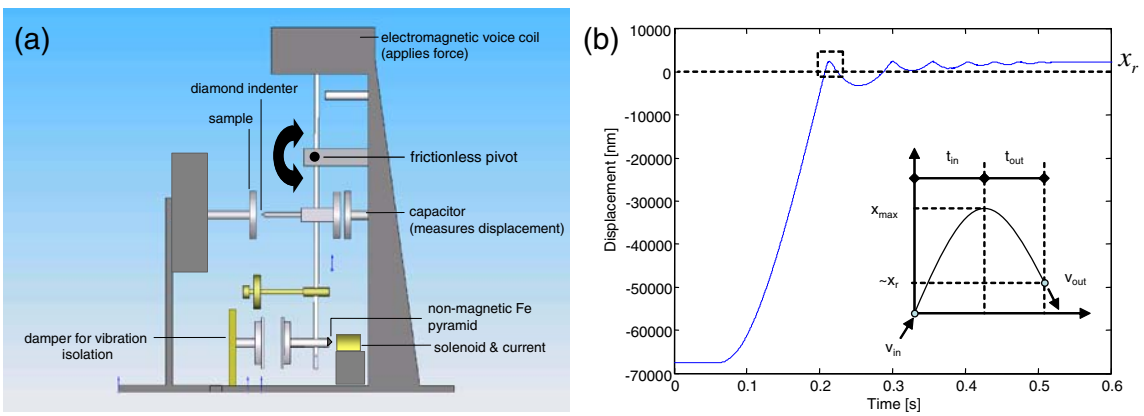

Fig. 1 (**a**) Experimental apparatus used to measure the impact response and corresponding impact energy dissipation. (**b**) Impulse response for 1100 aluminum at the lowest impact velocity considered, corresponding to an impact energy of ~ 50 nJ. *Inset*: A magnified version of the first upswing into the material showing test characteristics. Zero displacement represents the position of the undeformed surface

relative humidity (50%). Conventional contact loading is achieved by linearly increasing the coil current to a pre-determined maximum value after which it is linearly reduced. A continuous load/depth response is recorded from which quasi-static material properties are determined. Impulse contact loading is achieved via an additional hardware component. A material of low magnetic hysteresis (magnetically soft Fe) of conical geometry is secured to the bottom of the pendulum, as shown in Fig. 1(a), such that it can be attracted to and then held by a stationary solenoid. In impact mode, a constant current (which subsequently defines the kinetic energy of the pendulum) is first established and maintained in the pendulum loading coil. The solenoid is then energized to pull the indenter away from the specimen. To produce a single impact, the solenoid current is switched off, thereby releasing the pendulum to swing towards the specimen. The loading coil current remains constant throughout. From its initial stationary solenoid position, the indenter position x is monitored continuously as a function of time t, including the initial impact trajectory and the initial rebound from the material surface. Finally, we should note that the distribution of mass and stiffness of the pendulum was sufficient to avoid any modal vibrations that could be generated during impact (for the considered materials and impact velocities) to potentially interfere with the monitored displacement. Modal vibrations of the pendulum (~ 80 Hz resonance) may contribute to the measured impact response of the material for materials of higher quasistatic hardness, higher impact velocities, and/or blunter indenter geometries than considered herein. Increases in each of these experimental parameters would serve to dissipate less energy in the initial impact, and would be observed in the experimental output $x(t)$ as a departure from the smooth (sinusoidal) oscillation of the initial impact response.

Impact Measurements

The impact response of an elastoplastic material expected to exhibit minimal viscoelastic damping (1100 aluminum, density $\rho = 2.71$ g/cm^3 and elastic modulus $E = 70$ GPa) was measured. Specimens were polished to exhibit nm-scale surface roughness. For each impact velocity considered, at least five trials under identical conditions were conducted and analyzed. Pendulum displacement as a function of time $x(t)$ was recorded [see Fig. 1(b)], where $x = 0$ was known through calibration of the sample plane immediately prior to each impact. For the purposes of data analysis $t = 0$ was arbitrarily assigned as the time corresponding to $x = 0$, i.e., at the start of the first impact contact as shown in the inset of Fig. 1(b). For each experiment, the following data were monitored: impact and rebound velocities v_{in} and v_{out} corresponding to the initial impact, maximum depth $x_{\max}$, residual depth x_r, loading and unloading times t_{in} and t_{out} [see details in inset of Fig. 1(b)]. These extracted quantities are linked to material constants using a model developed below. The deviation in $x(t)$ among experiments for a given pendulum velocity and material sample was less than 5%. The resolution of displacement and force were 0.1 nm and 0.1 μN, respectively, and the displacement acquisition rate was 4000 pts/s, enabling impact loading with nanoscale spatial resolution over μs timescales (see Fig. 2).

Impact Model

The impact trajectory begins with the pendulum swinging towards the material surface, after the step-function decrease of the solenoid current that initiates pendulum motion. The kinetic energy of the pendulum increases until contact occurs with an impact force F_{im}. At $x = 0$ the probe contacts the material surface, and an additional resistance is felt by the pendulum due to the material $\mathcal{F}(x)$. During the indentation phase, deceleration occurs until the indenter comes to a complete halt at a maximum indentation depth (see Fig. 2). The kinetic energy of the pendulum has now been converted to reversible material deformation and/or irreversible dissipation via plastic deformation. The elastic energy

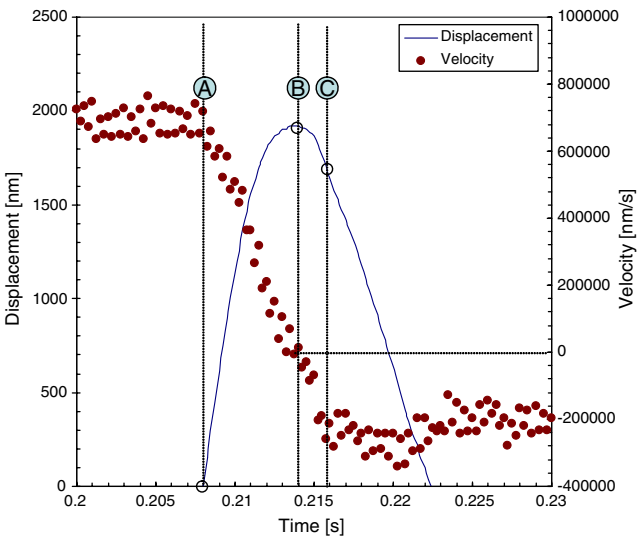

Fig. 2 Experimentally determined displacement-time curve for the first impact and the calculated corresponding velocity-time profile. The deceleration (A to B) and acceleration (B to C) phases of the motion are evident

stored in the material is recovered during the unloading portion of the curve, which also drives the indenter to rebound and accelerate away from the material. The proposed model involves the motion of the pendulum together with the influence of an additional resistance which begins as the indenter makes contact with the surface and increases as the indenter penetrates the material. This can be expressed mathematically as:

$$m\ddot{x} + c\dot{x} + kx + \mathcal{F}(x) = F_{\text{im}} \tag{1}$$

where m is the effective mass of the pendulum, c is the pendulum damping coefficient, mainly due to air damping, k is the pendulum spring stiffness, x is the indenter displacement relative to the sample surface, $\mathcal{F}(x)$ is the variable resistive force of the material, and F_{im} is the impact force required to impart the initial energy into the material. The resistive force $\mathcal{F}(x)$ varies according to:

$$\mathcal{F}(x) = \begin{cases} 0 & \text{if } x<0 \text{ and } \dot{x}>0 \\ \mathrm{C_{in}}x^2 & \text{if } x>0 \text{ and } \dot{x}>0 \\ \mathrm{C_{out}}x_{\max}x + (\mathrm{C_{in}} - \mathrm{C_{out}})x_{\max}^2 & \text{if } x>x_r \text{ and } \dot{x}<0 \\ 0 & \text{if } x<x_r \text{ and } \dot{x}<0 \end{cases} \tag{2}$$

where $\dot{x} > 0$ represents the positive velocity into the surface and $x_{\max}$ the maximum depth of indentation. The subscripts *in* and *out* signify the constant material quantities related to the loading and unloading portion of the indentation response. In equation (2) we assumed that the resistance of the material during indentation follows the quasi-static quadratic form $\sim \mathrm{C_{in}}x^2$, such that $\mathrm{C_{in}}$ is termed the resistance coefficient. For high velocities or time dependent material behavior this assumption breaks down and the strain rate sensitivity of the material and/or the kinetic energy of the targeted specimen should be considered in the analysis. We address this additional consideration explicitly in a separate paper, as this extension builds upon the rate-insensitive energy dissipation model developed herein [25].

The third condition in equation (2) describes a linear unloading portion of the $P-x$ response curve as normally used for quasi-static indentation analysis. Here, we define the initial slope or tangent of the unloading curve $dP/dx = \mathrm{C_{out}}x_{\max}$ (at $x = x_{\max}$) and we use the condition $P = \mathrm{C_{in}}x_{\max}^2$ at $x = x_{\max}$. The definition of dP/dx is chosen for dimensional consistency, and $\mathrm{C_{out}}$ is termed the recovery coefficient.

The constants c and k are characteristics of the pendulum and can be obtained from a pendulum calibration process described in Section Intrinsic Pendulum Damping. Equation (1) cannot be solved analytically, but a numerical solution can be obtained readily from algorithms in Matlab® or a similar language (not shown). The predictive capabilities of this model are demonstrated in the Impact Experiments section.

Results and Discussion

Intrinsic Pendulum Damping

It is important to identify the mass m, damping coefficient c, and spring constant k of the pendulum in the absence of material contact. These constants determine the free oscillation periodic time (T_D) of the pendulum, given by:

$$T_D = 2\pi/\omega_D = 2\pi\left[\omega_n\sqrt{1-\zeta^2}\right]^{-1} \tag{3}$$

T_D and c can, in principle, be obtained directly from the exponential decay of the pendulum amplitude with the pendulum freely swinging backwards and forwards ($x(t) \sim Ae^{-c/2mt}$). In practice, this time constant is obtained by producing an impact against a brass leaf spring and monitoring the subsequent pendulum motion. The stiffness of the leaf spring can be measured directly and taken into account. In particular, the damping ratio ζ for lightly damped systems can be calculated from the ratio of consecutive oscillation displacement peak heights from:

$$\zeta = \frac{1}{2\pi j}\ln\frac{x_i}{x_{i+j}} = \frac{c}{2m\omega_n} \tag{4}$$

The pendulum spring constant k was measured directly simply by hanging masses from the pendulum and measuring the resulting angular displacement ($k = 10$ N/m). The pendulum mass m was found by first identifying the pendulum resonant frequency (ω_r) with a spring inserted between the pendulum and the opposing sample holder. Oscillation over a wide range was carried out by means of a piezoelectric oscillator attached to the sample stage. After measuring the brass leaf spring stiffness ($k_s = 1866$ N/m) via a simple force-displacement test, the mass was calculated from:

$$m = \frac{k_s}{{\omega_r}^2} \tag{5}$$

In the present case, m of the pendulum was 0.21 kg. Equations (3) to (5) form a closed set of relations that allow the determination of the unknown impact parameters. Once these system constants were established, the damped harmonic oscillation of the pendulum, with the diamond in contact with a sample, could be analyzed to determine material-dependent quantities.

Figure 3 shows the free oscillation from which the intrinsic damping was calculated. From the consecutive peaks shown in this particular result, $\zeta = 2.42\%$. To summarize, the measured and calculated system constants were:

$$\begin{array}{lll} m = 0.21\ \text{kg} & c = 0.96\ \text{N.s/m} & k = 10\ \text{N/m} \\ \omega_n \simeq \omega_D \simeq 94.5\ \text{s}^{-1} & \zeta = 2.42\% & \varepsilon = 4.57\text{s/nm} \end{array} \qquad k_s = 1866\ \text{N/m} \tag{6}$$

Furthermore the $x(t)$-response was compared to the theoretical damped harmonic oscillator response [equation (24) in Appendix 1] assuming the above coefficients, showing excellent agreement (Fig. 3). As a final validation process, the peak heights of oscillations were fitted to the exponential decay functions $\pm Ae^{-c/2mt}$ and are shown in Fig. 3. These functions were found to be symmetric about the equilibrium position of the stationary pendulum ($x = 0$), indicating that the response can be adequately modeled using a damped harmonic oscillator, and that the observed decay of the oscillation amplitude over time is due solely to damping within the pendulum system.

Impact Experiments

Indentation impact experiments on 1100 aluminum were performed with impact velocities of 0.7, 1.0, 1.5 and 2.5 mm/s. Quasi-static indentation experiments were also performed to extract the material parameters (C_{in} and C_{out}) required to test the developed model [equation (1)]: $C_{in} = 6.5$ GPa and $C_{out} = 60$ GPa. The differences in response between impact on aluminum [Fig. 1(b)] and the free oscillations [Fig. 1(b)] are readily apparent, and underscore the unique mechanical response of elastoplastic materials. The most striking difference between these responses is the asymmetry induced by the material damping of the pendulum motion. The displacement or penetration depth x of the pendulum 'upswing' into the material is ~3 times smaller than that of the pendulum 'backswing', and the overall pendulum oscillation is not strictly periodic due to the different frequencies of oscillations that the pendulum experiences in the two domains. However, the envelope of this response continues to be a decaying exponential characterized by the pendulum and material characteristics. This damped oscillatory response due to material contact is shown in Fig. 1(b) for the specific case of aluminum under an initial impact energy of 50 nJ. As expected intuitively, aluminum strongly damps the amplitudes of oscillation exhibited by the pendulum, and also dissipates or damps the energy of the pendulum much faster than observed in the case of free-pendulum oscillations. The oscillations of the aluminum-pendulum system fall to the level of instrument resolution ($x \sim 1$ nm) after ~ 0.5 s. We pay particular attention to the first impact where the response is elastoplastic. Consecutive impacts involve the viscoelastic penetration of the indenter on an already deformed surface, which poses additional complexity to the analysis. The pendulum displacement over time for the first impact, given by the numerical solution of equation (1), is compared with our experimental data in Fig. 4. The almost perfect agreement between experiments and simulation for aluminum of known C_{in} and C_{out} confirms the robustness of our newly developed experimental method. The experimental data and

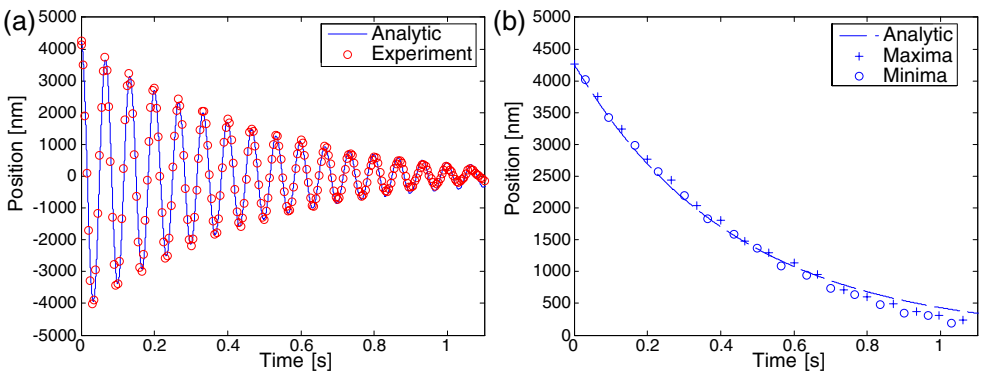

Fig. 3 Free oscillations of the pendulum-leaf spring system. The analytical solutions of damped harmonic motion (Appendix 1) were fitted to the experimentally obtained response to extract the pendulum intrinsic characteristics (**a**, **b**)

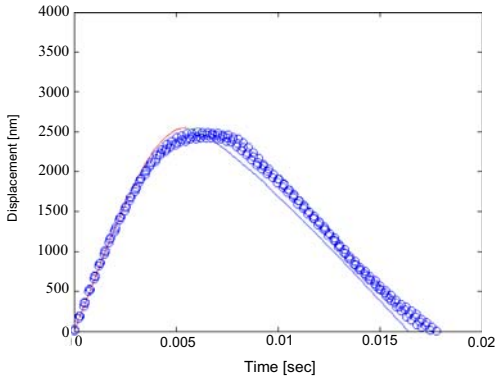

Fig. 4 Numerical simulation (*solid line*) vs experimental data (*circles*) of impact data on 1100 aluminum ($v_{in} = 0.68$ mm/s, impact energy =50 nJ)

modeling results for the different impact velocities are described in detail below.

Maximum depth $x_{\max}$, duration of impact t_{in}, and residual depth x_r

The equations presented in equations (1) and (2) cannot be solved analytically, but only numerically. In order to simplify the problem, we assume that the resistance posed by the material is significantly higher than the resistance associated with the pendulum friction and the restoring force such that equations (1) and (2) simplify to:

$$\text{Loading:} \ddot{x} + (\mathrm{C_{in}}/m)\, x^{a_{\mathrm{in}}-1} \simeq 0 \tag{7}$$

$$\text{Unloading:} \ddot{x} + (\mathrm{C_{out}}/m)\, x^{a_{\mathrm{out}}-1} + C_1 \simeq 0 \tag{8}$$

Andrews et al. [31] has previously demonstrated analytical and numerical results for impact indentation for a sharp indenter. One can extend their analytical solution to arbitrary geometry. Hence the maximum depth of penetration $x_{\max}$ is given by:

$$x_{\max} = \left(\frac{m a_{\mathrm{in}}}{2\mathrm{C_{in}}}\right)^{1/a_{\mathrm{in}}} v_{\mathrm{in}}{}^{2/a_{\mathrm{in}}} \tag{9}$$

where the coefficient a_{in} could be adjusted to accommodate other commonly employed indenter geometries: $a_{\mathrm{in}} = 2$ for a flat punch, $a_{\mathrm{in}} = 5/2$ for spherical indenter, and $a_{\mathrm{in}} = 3$ for sharp indenter (cone or pyramid). A sharp indenter is employed in this study, which indicates a quadratic resistance from the material in keeping with dimensional analysis[1] $\propto \mathrm{C_{in}} x^2$ [33]. In such a case where the loading portion is assumed quadratic, $a_{\mathrm{in}} = 3$, then equation (9) reduces to the one derived by Andrews et al. [31]:

$$x_{\max} = \left(\frac{3m v_{\mathrm{in}}{}^2}{2\mathrm{C_{in}}}\right)^{1/3} \tag{10}$$

The time of collision t_{in}, the residual depth x_r left on the surface of the specimen after the first impact, and the time required to lose contact ($P = 0$) t_{out}, can also be estimated through (see derivations in [31]):

$$t_{\mathrm{in}} = 1.4\left(\frac{3m}{2\mathrm{C_{in}} v_{\mathrm{in}}}\right)^{1/3} \tag{11}$$

$$x_r = x_{\max}\left(1 - \bar{\mathrm{C}}\right) \tag{12}$$

$$t_{\mathrm{out}} = \frac{\pi}{2}\sqrt{\left(\frac{m}{\mathrm{C_{out}} x_{\max}}\right)} \tag{13}$$

where the slope of the unloading curve was assumed equal to $dP/dx = \mathrm{C_{out}} x_{\max}$; $\mathrm{C_{out}}$ has the same units as $\mathrm{C_{in}}$; and $\bar{\mathrm{C}} = \mathrm{C_{out}}/\mathrm{C_{in}}$. Equations (10)–(13) provide access to material constants through experimentally obtained quantities.

Equation (10) suggests that the maximum indentation depth scales with the velocity as $x_{\max} \sim v_{\mathrm{in}}^{2/3}$. In fact, the depth of penetration is a direct function of the impact velocity and the resistance coefficient of the material, $\mathrm{C_{in}}$. As shown in Fig. 5(a) the comparable scaling of the experimental data support the scaling of the approximate analytic solution, equation (10). Furthermore the small deviation between the analytical solution and the numerical simulation is attributable to the additional resistance generated by the pendulum friction and damping during material oscillation, as well as the residual impact force left activated on the pendulum during the experiment.

Figure 5(b) shows residual depth x_r vs. $x_{\max}$ for the four different impact velocities. The experimental data

[1] This quadratic link between force and penetration depth was found to be a natural outcome of the dimensional analysis of sharp (conical or pyramidal) indentation, owing primarily to the geometric self-similarity of the problem [3, 32]. A series of theoretical [3] and computational [2, 33] studies elucidate this complicate contact mechanics problem and suggest that the square dependency persists irrespective of the material behavior, whether the solid behaves elastically [3] or inelastically, with strain hardening [32], or pressure sensitive [34] plasticity. It should, however, be noted that time-dependent material behavior can change the exponent of indentation to values lower than 2 [2].

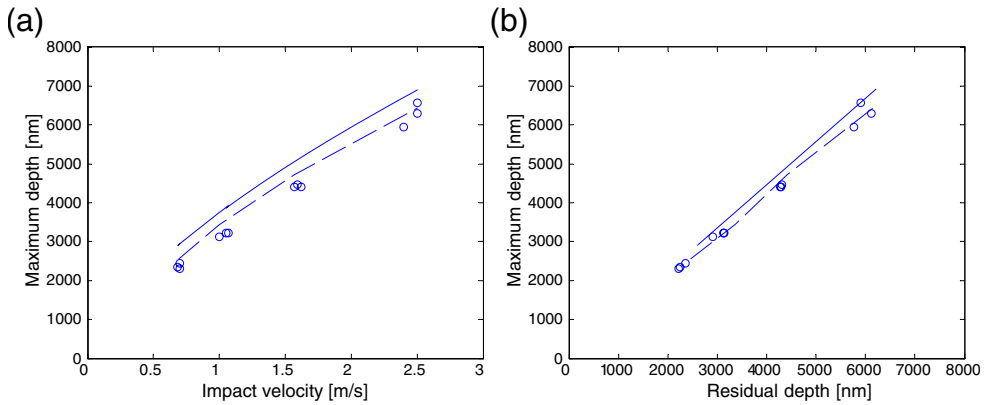

Fig. 5 (**a**) Maximum penetration depth as a function of impact velocity v_{in} for 1100 Al. Experimental data (*circles*); Analytical approximation (*solid line*) according to equation (10); Numerical simulation (*broken line*) according to equation (1). (**b**) Maximum penetration depth vs the residual depth on the surface of the specimen. Experimental data (*circles*); Analytical approximation (*solid line*) according to equation (12); Numerical simulation (*broken line*) according to equation (1)

is almost perfectly linear, as predicted by the one-dimensional model of Andrews et al. equation (12); $x_r = x_{\max}\left(1-\bar{C}\right) x_r/x_{\max}$ gives access to the impact resistance ratio $\bar{C}$: $x_r/x_{\max} = \left(1-\bar{C}\right)$. The recovery coefficient then follows from $C_{out} = \bar{C} \times C_{in}$. Quasistatic elastoplastic results presented by Giannakopoulos and Suresh [26], which were obtained using three dimensional finite element simulations, suggest that:

$$x_r/x_{\max} = 1 - d^* \frac{H}{E^*} = \frac{W_p}{W_t} \tag{14}$$

where d^* is a constant which depends on the indenter geometry ($d^* = 5$ for Vickers and $d^* = 4.7$ for Berkovich pyramids), H is the hardness of the material defined as the maximum load over the projected area of contact, E^* is the effective indentation modulus which is approximately equal to the plane stress modulus of the indented material $E/\left(1-\nu^2\right)$, while W_p and W_t are the plastic and total work of indentation with $W_t = \int_0^{x_{\max}} P(x)dx$. It is readily apparent that the depth ratio $x_r/x_{\max}$ and, as a consequence, the impact resistance ratio $\bar{C}$ are both proportional to the normalized plastic work:

$$\bar{C} = d^* \frac{H}{E} = 1 - \frac{W_p}{W_t} \tag{15}$$

Thus, $\bar{C}$ succinctly quantifies the energy dissipation under impact loading and provides a way to calculate the hardness to modulus ratio H/E for a material surface of interest, at a specified impact velocity. Furthermore, Fig. 6 shows the good agreement between the theoretical [equation (11)] and numerical prediction of the time of contact during this initial impact. For the given material and impact velocities, the contact duration is on the order of milliseconds and approaches the temporal resolution of this instrument ($\sim 0.25\mu s$).

In a reverse application, the recovery coefficient C_{out} and impact resistance ratio $\bar{C}$ can be evaluated from equation (12) or equation (13). Given the experimental observation that the residual depth is more accurately determined than the time of impact and recovery, we can evaluate $\bar{C}$ from direct measurements of x_r and $x_{\max}$. Once $\bar{C}$ is measured, the $H/E-$ ratio of the tested material can be calculated from equation (15). The $H/E-$ ratio is of particular importance, as this estimate of relative resistance to plastic and elastic deformation

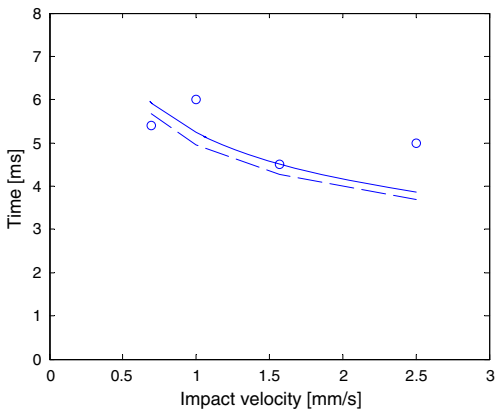

Fig. 6 Time of indentation as a function of impact velocity for 1100 Al. Experimental data (*circles*); Analytical approximation (*solid line*) according to equation (11); Numerical simulation (*broken line*) according to equation (1)

is predictive of elastic strain to failure, fracture toughness, and wear resistance [27].

Coefficient of restitution e

A useful quantity to express the energy loss during impact is the coefficient of restitution e defined as:

$$e = \left| \frac{v_{\text{out}}}{v_{\text{in}}} \right| \tag{16}$$

where v_{in} is the incident speed of the indenter and v_{out} the rebound speed. The value of e has been found useful in comparing the dissipation of energy during the collision of spheres, and has been experimentally measured for many objects, materials and surfaces [28]. The coefficient of restitution e of the pendulum-aluminum system was calculated by differentiating the measured displacement-time response and was found not to be a function of impact energy (i.e., of v_{in}) over the range of F_{im} considered herein. As illustrated in Fig. 7, e of the diamond indenter and aluminum system ranged from 0.38 to 0.42, showing statistically insignificant fluctuation over the tested velocity range. Generally, the coefficient of restitution is a measure of the elasticity of the collision. In fact, e can be recast in the form:

$$K = \left(\frac{1}{2} m v_{\text{in}}^2 - \frac{1}{2} m v_{\text{out}}^2 \right) / \frac{1}{2} m v_{\text{in}}^2 = 1 - e^2 \tag{17}$$

which is equivalent to the relative loss of kinetic energy dissipated during an impact, where $\frac{1}{2} m v_{\text{in}}^2$ and $\frac{1}{2} m v_{\text{out}}^2$ represent (approximately)[2] the total energy of the system before and after the collision. For an elastic collision where zero energy is lost, e will be equal to unity and K will be zero. It is therefore apparent that the coefficient of restitution is a measure of the material energy dissipation per impact. It is of interest to consider a relation to $\bar{C}$, another measure of energy dissipation, that comes from the residual depth rather than from an energy approach. Andrews et al. using

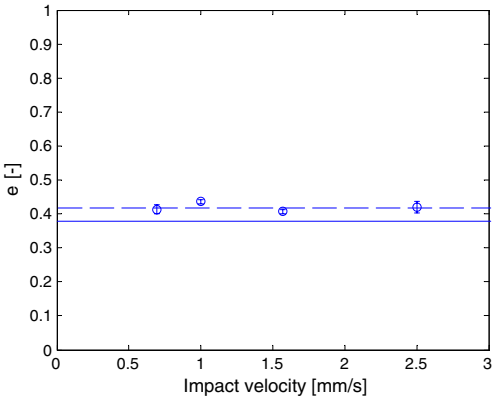

Fig. 7 Coefficient of restitution of 1100 aluminum for different impact velocities (*circles*). The approximate analytical solution (*solid line*) and the numerical simulation results (*broken line*) are also shown

the approximated solution derived a link between the outgoing velocity v_{out} and $\bar{C}$:

$$v_{\text{out}} = -v_{\text{in}} \left(\frac{3\bar{C}}{2} \right)^{1/2} \tag{18}$$

Given the definition of the coefficient of restitution in equation (16), we find the following relation:

$$e = \left(\frac{3\bar{C}}{2} \right)^{1/2} \tag{19}$$

which demonstrates that residual depth and the reduction in the velocity after the first impact are both a manifestation of the same energy dissipative mechanism. The numerical value of aluminum given by equation (19) is also shown in Fig. 7, and correlates well with our experimental data. Although e is not strictly equivalent to the coefficient of restitution of the material surface itself, but rather of the pendulum as damped by the material surface, it is clear that the dissipative capacity of the material dominates and e is robust and correlative with the mechanical properties ($C_{\text{in}}/C_{\text{out}}$) of a given solid under impact loading by another material comprising the indenter.

Impact hardness H_{imp}

Finally, the instantaneous resistance to impact deformation can be quantified as the impact hardness H_{imp}, which is defined (by analogy with static hardness) as equivalent to the absorbed energy of the material upon

[2]The energy input to the system by imparting it to its initial position $x(0)$ and giving it an initial velocity $\dot{x}(0)$ is the sum of the kinetic and potential energy:

$$T = \frac{1}{2} k [x(0)]^2 + \frac{1}{2} m [\dot{x}(0)]^2$$

During the period prior to first impact the energy can be calculated by considering the experimentally obtained $x(t)$ and $\dot{x}(t)$ in the above equation. When the pendulum first hits the material surface the potential energy of the system is zero and the total energy is equivalent of the kinetic energy $E_{\text{total}} = \frac{1}{2} m v_{in}^2$. During the rebound phase the material loses contact earlier approximately at $h = h_r$ and as a consequence the total energy is equivalent to $E_{\text{total}} = \frac{1}{2} m v_{out}^2 + \frac{1}{2} k h_r^2 \simeq \frac{1}{2} m v_{out}^2$ for the velocities considered herein.

the first impact, normalized by the estimated plastically deformed volume of that contact:

$$H_{imp} = \frac{\text{Energy of impact}}{\text{Volume of indentation}} \simeq \frac{\frac{1}{2}m({v_{\text{in}}}^2 - {v_{\text{out}}}^2)}{8.2x_r^3} \tag{20}$$

where v_{in} and v_{out} are determined as the time rate of change of x as the pendulum swings into and out of the sample surface, respectively, and the volume as a function of x_r is specific for a conical indenter of semi-apex angle equal to ~71° (consistent with the typical trigonal pyramid or Berkovich geometry utilized in most nanoindentation experiments and these impact experiments). Impulse hardness defined in this manner is essentially a measure of energy dissipation per unit volume of deformed material, or specific energy absorption. For systematic studies of material response as a function of impact velocity v, this definition could be further refined by considering the post-mortem indentation volume inclusive of sink-in or pile-up, in lieu of this idealized conical volume inferred from residual depth x_r. The impact hardness can be compared quantitatively with the quasistatic indentation hardness H_i that is determined from separate experiments in which the same indenter geometry is used to acquire a continuous load—depth $(P-h)$ profile upon a full loading cycle at a comparably slow rate (nm/s) intended to approximate the quasistatic conditions under which H_i is estimated from linear elastic contact mechanics:

$$H_i = \frac{P_{max}}{A_c} \tag{21}$$

where the area of contact at maximum load A_c, can be estimated according to the semi-empirical approach of Oliver and Pharr [1]. Here,

$$\begin{aligned} A_c &= 24.56{h_c}^2 = 24.56h_{max} - \epsilon\frac{P_{max}}{S} \\ &= 24.56\left(\frac{2}{\pi}(h_{max} - h_f) + h_f\right)^2 \end{aligned} \tag{22}$$

where P_{max} is maximum load, S is dP/dh or the tangent of the unloading response at P_{max}, and h_c, h_f, and h_{max} are the calculated contact depth, measured final depth, and measured maximum depth of contact at P_{max}, respectively.

Impulse hardness H_{imp} is similar in spirit to the dynamic hardness of metals [29, 36] employed as a means to infer yield strength under elevated loading rates, but differs in that the contact volume is significantly smaller and the hardness is inferred from measured energies and depths rather than from post-contact optical measurements of contact area A under a given load P. Provided that the depth of indentation is sufficient to avoid errors in A_c due to surface roughness or indenter geometry imperfections [30], we would expect dynamic hardness to be insensitive to impact velocity over this range [31]. In fact, we observe that dynamic hardness of 1100 aluminum agrees quite well with that measured under quasistatic (nm/s) displacement rates ($H_{imp} = 0.29 \pm 0.01$ GPa; $H_i = 0.27 \pm 0.01$ GPa). However, we note that this experimental approach is amenable to identification of materials or impact velocities/energies for which specific energy absorption is rate-dependent, and thus the impact hardness H_{imp} differs from the quasistatic indentation hardness H_i. Although the full treatment of this rate-dependent material response is beyond the scope of this paper [25], we note that under the same impact velocity (0.68 mm/s) and energy (250 nJ) applied to 1100 aluminum, specific energy absorption of gold was rate-dependent. Au annealed at 450°C for 10 min was softer than Au work-hardened via mechanical compression, as expected, but both Au samples exhibited $H_{imp} > H_i$ (Fig. 8).

This experimental and analytical approach can be applied to study the response of dissimilar materials (metals, ceramics, polymers, and composites thereof) and structural components (protective coatings-thin films, micrometer structures-MEMS etc.) to concentrated impact loading, including the mapping of specific energy dissipation over discrete locations in a structurally heterogeneous surface or composite. Note that this access to H_{imp} provides straightforward access to the ratio H/E. Increasing H/E indicates greater capacity of the material to absorb elastic energy (higher resilience), and ostensibly a greater resistance to deformation or wear under impact at the impact velocity of

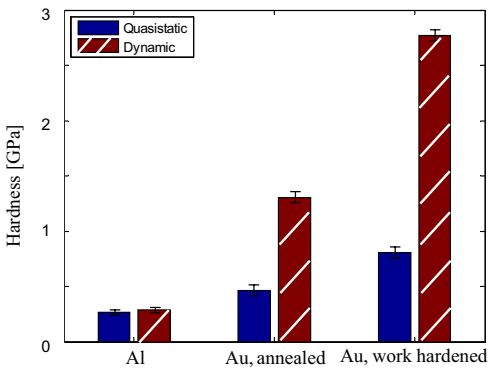

Fig. 8 Quasistatic and dynamic hardness values for 1100 Al, Au annealed at 450°C for 10 min, and Au work hardened via mechanical compression

interest [35]. We note that any new deformation physics exhibited by the material such as delamination, fracture, or strain rate sensitivity will cause deviation from the theoretical model predictions presented herein. The additional consideration of strain-rate sensitivity as anticipated in polymeric surfaces under impact is treated separately [25], as this extension requires thorough analysis of the strain-rate independent case outlined in this paper. The experimental data can be accompanied by numerical models such as finite element simulations to facilitate the extraction of meaningful mechanical properties consistent with the observed material response. In the absence of such brute-force computational simulation, the general qualitative metrics of energy dissipation (e and H_{imp}) will hold and can therefore be used to quantify the energy dissipation of a material surface under localized mechanical impact.

Conclusions

A novel indentation-enabled impact experimental approach and analysis detailed herein provides the means for dynamic characterization of material surfaces. This approach allows extraction of several unique metrics of material-dependent deformation in elastic-plastic materials, without assuming constitutive or phenomenological models *a priori*:

1. The indentation system is pendulum-based and dynamically tests material surfaces while continuously monitoring the pendulum displacement response by imparting an electromagnetically triggered mechanical impact via indenter contact. The instrument resolution is sufficient to enable mapping of the energy dissipation capacity of discrete material volumes across the surface of or through the thickness of a structurally heterogenous material.
2. The impact indentation responses were obtained for 1100 aluminum for four different velocities in the mm/s range. The profiles were in very good agreement with a proposed mechanical model, confirming the robustness of the experimental technique.
3. Coefficient of restitution e and the ratio of impact coefficients $\bar{C}$ for 1100 aluminum were found to be independent of impact velocity and unique characteristics of this model material. This demonstrates that the relative dissipation of energy during impact W_p/W_t is independent of the initial velocity, over the range considered, and is primarily driven by the materials and geometry of the surfaces under impact contact.
4. The impact hardness H_{imp} or specific energy absorption was found to correlate well with the static hardness of indentation for 1100 aluminum over the nm/s to mm/s range of displacement rates considered. Rate-dependent energy dissipation as the one observed in work hardened and annealed Au can be identified through this experimental approach. This topic is treated separately through an extension of the rate-independent model herein [25], as would be of interest to metals and ceramics under impact or to viscoelastoplastic polymers and composites.

Acknowledgements KJVV gratefully acknowledges partial support from the 3M Innovation Fund, and CAT acknowledges support through the National Defense Science and Engineering Graduate Fellowship program.

Appendix 1

Damped Harmonic Motion

When the pendulum travels away from the surface, the oscillations can be well described using free damped harmonic motion (DHM). In this kind of motion a restoring force kx attempts to bring the displaced body of mass m back to its equilibrium position while a frictional force proportional to the velocity of the pendulum body $c\dot{x}$ restrains the motion and dissipates energy with time:

$$m\ddot{x} + c\dot{x} + kx = 0 \tag{23}$$

Normalizing equation (23) by the body mass m we obtain:

$$\ddot{x} + \varepsilon\dot{x} + \omega_n^2 x = 0 \tag{24}$$

where

$$\varepsilon = 2\varsigma\omega_n = \frac{c}{m} \tag{25}$$

$$\zeta = \frac{c}{2m\omega_n} = \frac{c}{c_{cr}} \tag{26}$$

$$\omega_n = \sqrt{k/m} \tag{27}$$

A solution to the DHM is provided in cases where damping is weak ($c < c_{cr}$ or $\zeta < 1$). Given the initial conditions:

$$\text{at } t = 0\text{: } x = x(0)\,;\ \dot{x} = \dot{x}(0) \tag{28}$$

the now classical solution of equation (24) in time is:

$$x(t) = e^{-\varsigma\omega_n t}\left[x(0)\cos(\omega_D t) + \frac{\dot{x}(0) + \varsigma\omega_n x(0)}{\omega_D}\sin(\omega_D t)\right] \tag{29}$$

where the damped harmonic frequency ω_D relates to the undamped one through:

$$\omega_D = \omega_n\sqrt{1-\zeta^2} \tag{30}$$

The response is periodic, but the frequency of the oscillations is smaller compared to the undamped frequency (ω_n) and the amplitude of the oscillations is gradually decreasing. The time needed for the pendulum to leave the material the m−th time with speed $v_{\text{out, m}}$ and reenter the surface with velocity $v_{\text{in, m+1}}$ is equivalent to half a cycle, i.e. $T_D/2 = \pi/\omega_D$. Letting $\lambda = \varepsilon\pi/2\omega_D$ we find:

$$v_{\text{in, m+1}} = v_{\text{out,m}}e^{-\lambda} \tag{31}$$

Furthermore differentiating equation (29) with respect to t and setting $t = \pi/(2\omega_D)$ (quarter cycle) we find that:

$$v_{\text{in, m+1}} = x(0)\,\omega_D - \frac{\varepsilon}{2}\frac{\dot{x}(0)}{\omega_D} \tag{32}$$

Equation (32) allows one to calculate the initial impact velocity of the pendulum given the initial boundary conditions ($x(0)$ and $\dot{x}(0)$). Finally the m-th amplitude of oscillation for which $x = x_{\min}$ then follows as:

$$x_{\min} = \frac{v_{\text{out,m}}}{\omega_D}e^{-\lambda/2} \tag{33}$$

References

1. Oliver WC, Pharr GM (2004) Measurement of hardness and elastic modulus by instrumented indentation: advances in understanding and refinements to methodology. J Mater Res 19:3–20
2. Cheng YT, Cheng CM (2004) Scaling, dimensional analysis, and indentation measurements. Mater Sci Eng R 44:91–149
3. Sneddon IN (1965) The relation between load and penetration in the axisymmetric boussinesq problem for a punch of arbitrary profile. Int J Eng Sci 3:47–57
4. Binnig G, Quate C, Gerber C (1986) Atomic force microscope. Phys Rev Lett 56:930–933
5. Beake BD, Goodes SR, Smith JF, Gao F (2004) Nanoscale repetitive impact testing of polymer films. J Mater Res 19:237–247
6. Kolsky H (1949) An investigation of the mechanical properties of materials at very high rates of loading. Proc Phys Soc B 62:676–700
7. Wilkins M, Guinan M (1973) Impact of cylinders on a rigid boundary. J Appl Phys 44:1200–1206
8. Davis C, Hunter S (1960) Assesment of the strain-rate sensitivity of metals by indentation with conical indenters. J Mech Phys Solids 8:235–254
9. Sughash G, Zhang H (2007) Dynamic indentation response of ZrHf-based bulk metallic glasses. J Mater Res 22:478–485
10. Tirupataiah Y, Sundararajan G (1991) A dynamic indentation technique for the characterization of the high-strain rate plastic-flow behavior of ductile metals and alloys. J Mech Phys Solids 39:243–271
11. Johnson KL (1985) Contact mechanics. Cambridge University Press, Cambridge
12. French AP (1971) Vibrations and waves. W.W. Norton, New York
13. Neideck K, Franzel W, Grau P (1999) Dynamic ball hardness tests on polymers. J Macromol Sci B 38:669–680
14. Bhattacharya AK, Nix WD (1988) Analysis of elastic and plastic-deformation associated with indentation testing of thin-films on substrates. Int J Solids Struct 24:1287–1298
15. Nix WD (1997) Elastic and plastic properties of thin films on substrates: nanoindentation techniques. Mater Sci Eng A Struct 234:37–44
16. Saha R, Nix WD (2002) Effects of the substrate on the determination of thin film mechanical properties by nanoindentation. Acta Mater 50:23–38
17. Savage MF, Tatalovich J, Zupan M, Hemker KJ, Mills MJ (2001) Deformation mechanisms and microtensile behavior of single colony ti-6242si. Mater Sci Eng A Struct 319: 398–403
18. Greer JR, Nix WD (2005) Size dependence of mechanical properties of gold at the sub-micron scale. Appl Phys A Mater 80:1625–1629
19. Tadmor EB, Miller R, Phillips R, Ortiz M (1999) Nanoindentation and incipient plasticity. J Mater Res 14:2233–2250
20. Van Vliet KJ, Li J, Zhu T, Yip S, Suresh S (2003) Quantifying the early stages of plasticity through nanoscale experiments and simulations. Phys Rev B 67:104105
21. Lilleodden ET, Zimmerman JA, Foiles SM, Nix WD (2003) Atomistic simulations of elastic deformation and dislocation nucleation during nanoindentation. J Mech Phys Solids 51:901–920
22. Minor AM, Lilleodden ET, Stach EA, Morris JW (2004) Direct observations of incipient plasticity during nanoindentation of al. J Mater Res 19:176–182
23. Fago M, Hayes RL, Carter EA, Ortiz M (2004) Density-functional-theory-based local quasicontinuum method: prediction of dislocation nucleation. Phys Rev B 70:100102(R)
24. Lund AC, Hodge AM, Schuh CA (2004) Incipient plasticity during nanoindentation at elevated temperatures. Appl Phys Lett 85:1362–1364
25. Constantinides G, Tweedie CA, Holbrook DM, Barragan P, Smith JF, Van Vliet KJ (2008) Quantifying deformation and energy dissipation of polymeric surfaces under localized impact. Mater Sci Eng A 489:403–412
26. Giannakopoulos AE, Suresh S (1999) Determination of elastoplastic properties by instrumented sharp indentation. Scr Mater 40:1191–1198
27. Ashby MF, Jones DRH (1998) Engineering materials 2, 2nd edn. Butterworth Heineman, Oxford
28. Cross R (1999) The bounce of a ball. Am J Phys 67:222–227
29. Tabor D (2000) The hardness of metals, 2nd edn. Oxford classical texts in the physical sciences. Oxford University Press, Oxford
30. Constantinides G, Silva ECCM, Blackman GS, Van Vliet KJ (2007) Dealing with imperfection: quantifying potential

length scale artefacts from nominally spherical indenter probes. Nanotechnology 18:305503
31. Andrews EW, Giannakopoulos AE, Plisson E, Suresh S (2002) Analysis of the impact of a sharp indenter. Int J Solids Struct 39:281–295
32. Cheng YT, Cheng CM (1998) Scaling approach to conical indentation in elastic-plastic solids with work hardening. J Appl Phys 84:1284–1291
33. Dao M, Chollacoop N, Van Vliet KJ, Venkatesh TA, Suresh S (2001) Computational modeling of the forward and reverse problems in instrumented sharp indentation. Acta Mater 49:3899–3918
34. Ganneau FP, Constantinides G, Ulm F-J (2006) Dual-indentation technique for the assessment of strength properties of cohesive-frictional materials. Int J Solids Struct 43:1727–1745
35. Lima MM, Godoy C, Modenesi PJ, Avelar-Batista JC, Davison A, Matthews A (2004) Coating fracture toughness determined by Vickers indentation: an important parameter in cavitation erosion resistance of WC–Co thermally sprayed coatings. Surf Coat Technol 177–178:489–496
36. Marshall BM, Evans AG (1983) Measurement of dynamic hardness by controlled sharp-projectile impact. J Am Ceram Soc 66:580–585